nature climate change

LETTERS

PUBLISHED ONLINE: 10 APRIL 2017 | DOI: 10.1038/NCLIMATE3262

An observation-based constraint on permafrost loss as a function of global warming

S. E. Chadburn[1,2*], E. J. Burke[3], P. M. Cox[2], P. Friedlingstein[2], G. Hugelius[4] and S. Westermann[5]

Permafrost, which covers 15 million km^2 of the land surface, is one of the components of the Earth system that is most sensitive to warming[1,2]. Loss of permafrost would radically change high-latitude hydrology and biogeochemical cycling, and could therefore provide very significant feedbacks on climate change[3–8]. The latest climate models all predict warming of high-latitude soils and thus thawing of permafrost under future climate change, but with widely varying magnitudes of permafrost thaw[9,10]. Here we show that in each of the models, their present-day spatial distribution of permafrost and air temperature can be used to infer the sensitivity of permafrost to future global warming. Using the same approach for the observed permafrost distribution and air temperature, we estimate a sensitivity of permafrost area loss to global mean warming at stabilization of $4.0^{+1.0}_{-1.1}$ million km^2 °C^{-1} (1σ confidence), which is around 20% higher than previous studies[9]. Our method facilitates an assessment for COP21 climate change targets[11]: if the climate is stabilized at 2 °C above pre-industrial levels, we estimate that the permafrost area would eventually be reduced by over 40%. Stabilizing at 1.5 °C rather than 2 °C would save approximately 2 million km^2 of permafrost.

Permafrost, defined as ground that remains at or below 0 °C for two or more consecutive years, underlies 24% of the land in the Northern Hemisphere[12]. Under recent climate warming, permafrost has begun to thaw, causing changes in ecosystems and impacting northern communities, for example through collapse of roads and buildings as the ground becomes unstable[13]. Large quantities of carbon are stored in organic matter in permafrost soils[14], which starts to decompose when the permafrost thaws, resulting in the emission of greenhouse gases such as carbon dioxide and methane. In the future, carbon release from permafrost thaw may have a significant impact on the Earth's climate[6]. Due to its global importance, numerous modelling studies have assessed the rate of permafrost thaw under future climate warming[9,10,15,16]. However, despite progress in process-based modelling on local and regional scales, for example, ref. 17, a lack of data availability and model limitations mean that permafrost is still poorly simulated in global climate models, where the historical simulations show a present-day permafrost area anywhere between 0.1 and 1.8 times the size of that observed[9]. Models often have shallow soil columns, a limited representation of soil properties, inadequate snow thermal and physical dynamics and other missing processes[9]. Here we present a projection of large-scale permafrost thaw that is based on observations, avoiding model bias, and accounting for observational uncertainty.

Our approach is based on using the relationship between mean annual air temperature (MAAT) and permafrost occurrence to estimate permafrost extent. Permafrost is not exclusively determined by air temperature, being strongly influenced by landscape features such as topography, soil thermal properties, snow depth and hydrology[18]. Nonetheless, it is possible to construct a broad relationship between MAAT and the presence of permafrost, defined in terms of the probability of finding permafrost at a given air temperature[19]. Averaged over broad spatial scales, probability translates to the areal fraction underlain by permafrost. We derived a MAAT–permafrost relationship using a robust approach that integrates the spatial distribution of permafrost from the International Permafrost Association (IPA) map of permafrost in the Northern Hemisphere[20].

The observation-based IPA map defines the spatial boundaries of the permafrost zones: continuous, >90% coverage; discontinuous, 50–90% coverage; sporadic, 10–50% coverage; isolated patches, 0–10% coverage. We took the air temperatures at the spatial permafrost boundaries and fitted them against the respective permafrost fractions. The resulting relationship between MAAT and permafrost fraction is shown in Fig. 1a. We also provide a plausible range, which covers different sources of uncertainty. Firstly, the range of air temperatures for a given permafrost fraction indicates variability due to large-scale differences in snow depth, soil moisture, landscape type and so on; secondly, uncertainties in the IPA map are incorporated by including air temperatures from 100 km either side of each boundary. Detailed evaluation of this relationship by validation against local field data and regional modelling suggests that it is robust (see Supplementary Information).

We used this relationship between MAAT and permafrost to reconstruct the IPA permafrost map from WATCH reanalysis air temperatures (using the 1960–1990 period, consistent with the IPA-map observational window)[21,22] (Fig. 1b,c). The estimated permafrost area is 15.5 million km^2 using this technique (12.0–18.2 million km^2 using minimum/maximum curves), which compares well to 15.0 million km^2 from observations[20] (12.6–18.4 million km^2). A spatial correlation between observed and estimated permafrost extent has an r^2 value of 0.85. Note that this area refers to the actual area of permafrost, whereas the larger value given in ref. 12 includes the total area of all permafrost zones (for example, including the whole sporadic zone, of which only a small fraction is actually permafrost).

Figure 1d,e shows the maximum and minimum permafrost distributions according to the limiting curves on Fig. 1a. It is clear that any major discrepancy between the observed distribution and our estimate is covered by the maximum and minimum distributions (see also Supplementary Fig. 8). One of the major causes of such discrepancies is snow, which insulates the ground in winter[23]. We included the influence of factors such as snow and

[1]University of Leeds, School of Earth and Environment, Leeds LS2 9JT, UK. [2]University of Exeter, College of Engineering, Mathematics and Physical Sciences, Exeter EX4 4QF, UK. [3]Met Office Hadley Centre, FitzRoy Road, Exeter EX1 3PB, UK. [4]Stockholm University, Department of Physical Geography, 106 91 Stockholm, Sweden. [5]University of Oslo, Department of Geosciences, PO Box 1047 Blindern, NO-0316 Oslo, Norway.
*e-mail: s.e.chadburn@exeter.ac.uk

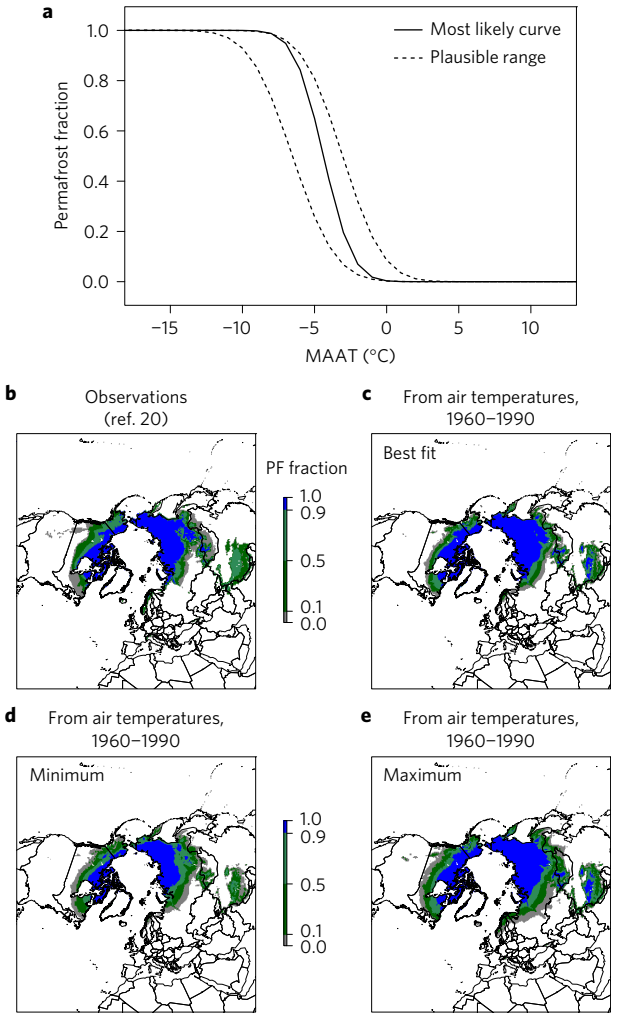

Figure 1 | Defining the spatial distribution of observed permafrost as a function of observed air temperature. a, Relationship between MAAT and permafrost fraction or probability. The central curve gives the most likely value, with upper and lower curves giving the plausible range. See Supplementary Fig. 1 for parameter values. **b**–**e**, Permafrost distribution estimated from reanalysis air temperatures and relationships in **a** (central curve (**c**), lower curve (**d**), upper curve (**e**)) validated against the IPA map (**b**)[20].

ground thermal properties in the limiting curves instead of spatially resolving them[15,24], to account for the full range of uncertainties in future projections.

We applied this relationship (Fig. 1a) to make projections of future permafrost extent. Our approach calculates the committed permafrost distribution for each global mean temperature. During a period of warming, the actual changes in permafrost area will lag behind this quasi-equilibrium state, due to the long timescale of warming for the deep ground. However, our analysis has high relevance to international climate negotiations, which are framed in terms of climate stabilization. We can, for example, estimate the relative impacts of stabilizing at 1.5 °C or 2 °C above pre-industrial levels[11].

Coupled models provide the best available indication of whether the relationship between MAAT and permafrost will fundamentally shift in the future (for example, if there is a pan-Arctic-scale change in snow depth relative to air temperature). We therefore test this using the CMIP5 (Coupled Model Intercomparison Project Phase 5) climate model ensemble[25], which provides a large data set of coupled simulations. For each model we derive a model-specific MAAT–permafrost relationship from the historical simulation (Supplementary Fig. 3). The robustness of our approach depends on the extent to which this relationship between permafrost area and air temperature remains consistent under climate change. The transferability of the MAAT–permafrost relationship was assessed by comparing the relationship derived from the models for the historical period 1960–1990, to that for the period 2270–2300 (Supplementary Fig. 4). The MAAT–permafrost curves for these two periods are generally very similar, and always within our uncertainty bounds. This is one of the main reasons that our approach is robust, as it is valid in every case despite the fact that the models differ in their representation of the key processes and in the details of their projections. We then estimated the future permafrost area, using the historical MAAT–permafrost relationships and future air temperatures from each model (Fig. 2a), including nine coupled climate models used in the latest IPCC (Intergovernmental Panel on Climate Change) assessment[26], and two different emission scenarios. The area is accurately estimated in every case.

We applied the same technique using the 'true' observationally derived MAAT–permafrost curve (Fig. 1a) to make projections of future permafrost area that are constrained by observations. To be independent of specific climate models and emission scenarios, we reduced the future air temperature changes down to just two variables: global mean warming, and Arctic amplification as a function of latitude. For this we used a pattern-scaling technique, in which air temperatures are increased by the global mean warming multiplied by the Arctic amplification. Arctic amplification is the phenomenon caused by changing surface albedo due to the melting of snow and ice, in which air temperatures in the Arctic warm approximately twice as fast as the global mean[26]. We estimate the amplification factor as a function of latitude, from the observed historical warming trend (1936–2012), using the WATCH reanalysis air temperature data[21,22] (Supplementary Table 2). The observed amplification factor differs substantially from models[27] (Supplementary Fig. 5), which is a good reason for using this approach rather than simulated future air temperatures (see Methods for further discussion).

The CMIP5 models were used to test the consistency of this technique. Using the same information from the models that is available for the real world (Arctic amplification derived from historical simulations (1936–2012), and global mean warming), we estimate the future air temperatures for each model. From these we again use the model-specific MAAT–permafrost relationships to estimate future permafrost area. This gives projections of future permafrost area that agree with the simulated permafrost areas within the uncertainty for all models (Fig. 2b).

We can therefore apply our methodology using observational data alone, namely observed present-day air temperature, historical Arctic amplification, and the observed MAAT–permafrost relationship (Fig. 1a), to estimate global permafrost loss for a given level of future global warming.

Using our approach, the loss of permafrost under stabilization, as a function of the global mean warming, is $4.0^{+1.0}_{-1.1}$ million km^2 °C^{-1} (note that all uncertainties are quoted at 1σ level). Under a 1.5 °C stabilization scenario, $4.8^{+2.0}_{-2.2}$ million km^2 of permafrost would be lost compared with the 1960–1990 baseline (corresponding to the IPA map, Fig. 1b), and under a 2 °C stabilization we would lose $6.6^{+2.0}_{-2.2}$ million km^2, over 40% of the present-day permafrost area. Therefore, stabilizing at 1.5 °C rather than 2 °C could potentially prevent approximately 2 million km^2 of permafrost from thawing. The loss of permafrost with warming is shown on Fig. 3 for a wide range of scenarios. Our results indicate that for the high warming scenarios (5 or 6 °C above pre-industrial—similar to the warming in RCP8.5 by 2100[26]), the vast majority of permafrost will thaw, leaving only 0.3–3.1 million km^2 under 5 °C of warming and 0.0–1.5 million km^2 under 6 °C. Even accounting for the

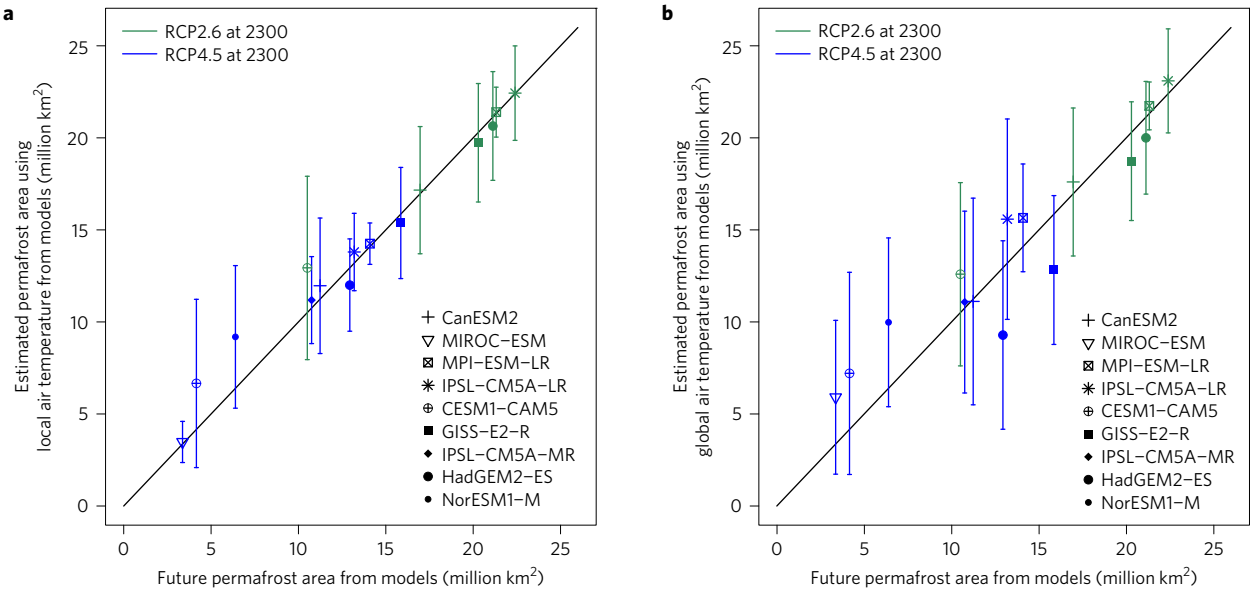

Figure 2 | Comparison of our estimate of global permafrost area with that simulated by the CMIP5 models (stabilization runs at 2300). a, Using local air temperature from the models and the model-specific MAAT–permafrost relationships. **b**, Using global temperature from the models, Arctic amplification from each model's historical simulation and the MAAT–permafrost relationships. Error bars show 2σ confidence.

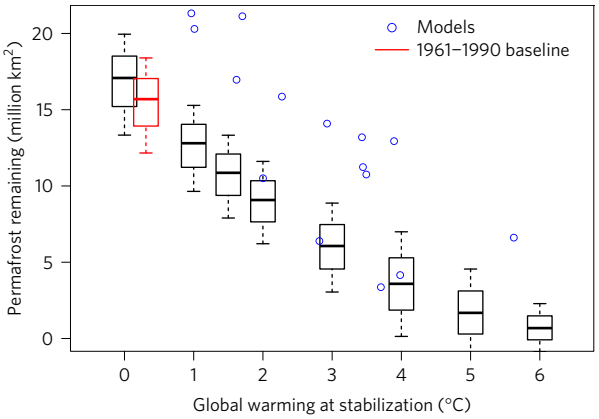

Figure 3 | Relationship between global warming stabilization scenario and remaining permafrost area using our approach. Boxes show 1σ and whiskers show 2σ uncertainty bounds. Zero warming corresponds to pre-industrial climate (1850–1900 average). The red box corresponds to the time frame of the IPA permafrost map (Fig. 1b). The 'model' points represent individual CMIP5 climate model stabilization simulations (permafrost area at 2300).

uncertainties due to heterogeneity in air temperature, snow and so on, we have greatly reduced the range from the unconstrained model ensemble (shown on Fig. 3).

Our approach also enables a broad spatial assessment of permafrost vulnerability, which is difficult with Earth system models due to problems with their simulation of the current permafrost distribution[9]. Figure 4 shows the estimated spatial pattern of high-latitude permafrost historically (1960–1990), and the range of the zonal boundaries under 1.5 °C stabilization (Fig. 4a) and 2 °C stabilization (Fig. 4b). Thawing permafrost has direct impacts on people and infrastructure in the areas where it thaws. Thirty-five million people live in the permafrost zone[28,29], including in three cities (population >100,000) built on continuous permafrost (marked on Fig. 4). These cities, for example, would most likely transition to the discontinuous permafrost zone under 2 °C of warming, putting their infrastructure at risk. Hydrological impacts vary with the depth of thaw but would include localized ground collapse, lake formation and soil drainage. Note that due to the nature of our approach, only large-scale spatial patterns of permafrost thaw are considered.

Previous estimates of permafrost sensitivity were generally given in terms of high-latitude warming, rather than global warming. Previous published values are equivalent to 3.3 ± 1.2 million km^2 °C^{-1}, based on the CMIP5 model simulations[9], and 1.8–2.6 million km^2 °C^{-1} based on an ensemble of offline model runs[16]. These are smaller than our value of $4.0^{+1.0}_{-1.1}$ million km^2 °C^{-1} (although they fall within $1–2\sigma$ of our estimate). The published values[9,16] are derived from transient simulations, so the difference may be partly due to the transient effect, where permafrost thaw 'lags' behind the climate warming, especially under scenarios such as RCP8.5 where the air temperature changes very quickly. Indeed, a study using equilibrium permafrost models driven by CMIP5 model output[10] showed that the equilibrium response is typically 25–38% greater than the transient response, and in some models the difference was even larger (up to 70%). The major advantage of the approach adopted here is that committed permafrost loss, along with its uncertainty, can be estimated for any policy-relevant global warming scenario.

We estimate the committed permafrost loss over the whole twentieth century to be $3.4^{+2.2}_{-2.3}$ million km^2 (until 2003–2012[26]). Some of this committed change will not yet be observable, because of the lag between the equilibrium and transient response. However, our estimate of permafrost sensitivity to warming is consistent with observations of changes in near-surface permafrost, which are expected to be much closer to equilibrium (see Supplementary Figs 6 and 7 and Supplementary Discussion). There may be longer-term transient effects, but these are relatively small (see Supplementary Fig. 2).

This is the first study to quantify permafrost loss under policy-relevant climate stabilization scenarios, defined by the global warming. In particular we take an approach that is based on observations and independent of climate model projections, reducing the problem of future sensitivity down to only two key quantities: Arctic amplification and global mean temperature change. Furthermore, our constraint includes a comprehensive uncertainty bound, specifically giving a sensitivity to global

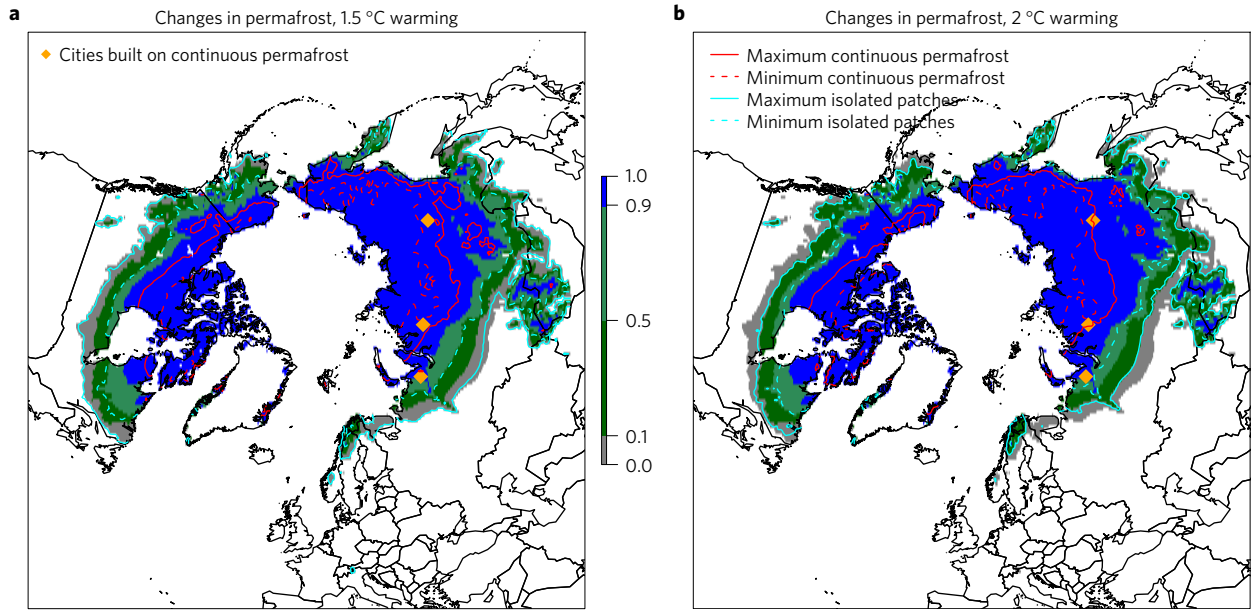

Figure 4 | Changes in spatial patterns of permafrost under future stabilization scenarios. a,**b**, The shaded areas show estimated historical permafrost distribution (1960–1990), and contours show the plausible range of zonal boundaries under 1.5 °C stabilization (**a**) and under 2 °C stabilization (**b**).

warming of $4.0^{+1.0}_{-1.1}$ million km^2 °C^{-1} at the 1σ level. This provides an important benchmark for process-based global modelling. Using our approach we have analysed the difference between 1.5 and 2 °C stabilization, and shown that the committed permafrost loss is nearly 30% smaller at the lower stabilization target, with relevance to climate negotiations surrounding the Paris Agreement[11].

Methods

Methods, including statements of data availability and any associated accession codes and references, are available in the online version of this paper.

Received 15 August 2016; accepted 8 March 2017; published online 10 April 2017

References

1. Romanovsky, V. *et al*. in *Arctic Report Card 2013* 131–136 (NOAA Arctic Program, 2013); ftp://ftp.oar.noaa.gov/arctic/documents/ArcticReportCard_full_report2013.pdf
2. Romanovsky, V., Burgess, M., Smith, S., Yoshikawa, K. & Brown, J. Permafrost temperature records: indicators of climate change. *Eos* **83,** 589–594 (2002).
3. Grosse, G., Goetz, S., McGuire, A. D., Romanovsky, V. E. & Schuur, E. A. G. Changing permafrost in a warming world and feedbacks to the Earth system. *Environ. Res. Lett.* **11,** 040201 (2016).
4. Schaefer, K., Lantuit, H., Romanovsky, V. E., Schuur, E. A. G. & Witt, R. The impact of the permafrost carbon feedback on global climate. *Environ. Res. Lett.* **9,** 085003 (2014).
5. Schneider von Deimling, T. *et al*. Estimating the near-surface permafrost-carbon feedback on global warming. *Biogeosciences* **9,** 649–665 (2012).
6. Schuur, E. A. G. *et al*. Climate change and the permafrost carbon feedback. *Nature* **520,** 171–179 (2015).
7. MacDougall, A. H., Avis, C. A. & Weaver, A. J. Significant contribution to climate warming from the permafrost carbon feedback. *Nat. Geosci.* **5,** 719–721 (2012).
8. Burke, E. J., Hartley, I. P. & Jones, C. D. Uncertainties in the global temperature change caused by carbon release from permafrost thawing. *Cryosphere* **6,** 1063–1076 (2012).
9. Koven, C. D., Riley, W. J. & Stern, A. Analysis of permafrost thermal dynamics and response to climate change in the CMIP5 Earth System Models. *J. Clim.* **26,** 1877–1900 (2013).
10. Slater, A. G. & Lawrence, D. M. Diagnosing present and future permafrost from climate models. *J. Clim.* **26,** 5608–5623 (2013).
11. *Adoption of The Paris Agreement* FCCC/CP/2015/L.9/Rev.1 (UNFCCC, 2015); http://unfccc.int/resource/docs/2015/cop21/eng/l09r01.pdf
12. Zhang, T., Barry, R. G., Knowles, K., Heginbottom, J. A. & Brown, J. Statistics and characteristics of permafrost and ground-ice distribution in the Northern Hemisphere. *Pol. Geogr.* **23,** 132–154 (1999).
13. Schaefer, K., Lantuit, H., Romanovsky, V. & Schuur, E. A. G. *Policy Implications of Warming Permafrost* (United Nations Environment Programme, 2012); http://wedocs.unep.org/handle/20.500.11822/8533
14. Hugelius, G. *et al*. Estimated stocks of circumpolar permafrost carbon with quantified uncertainty ranges and identified data gaps. *Biogeosciences* **11,** 6573–6593 (2014).
15. Anisimov, O. A. & Nelson, F. E. Permafrost zonation and climate change in the Northern Hemisphere: results from transient general circulation models. *Climatic Change* **35,** 241–258 (1997).
16. Chadburn, S. E. *et al*. Impact of model developments on present and future simulations of permafrost in a global land-surface model. *Cryosphere* **9,** 1505–1521 (2015).
17. Westermann, S., Østby, T. I., Gisnås, K., Schuler, T. V. & Etzelmüller, B. A ground temperature map of the North Atlantic permafrost region based on remote sensing and reanalysis data. *Cryosphere* **9,** 1303–1319 (2015).
18. Jorgenson, M. *et al*. Resilience and vulnerability of permafrost to climate change. *Can. J. For. Res.* **40,** 1219–1236 (2010).
19. Gruber, S. Derivation and analysis of a high-resolution estimate of global permafrost zonation. *Cryosphere* **6,** 221–233 (2012).
20. Brown, J., Ferrians, O. J. Jr, Heginbottom, J. & Melnikov, E. *Circum-Arctic Map of Permafrost and Ground Ice Conditions* (National Snow and Ice Data Center, 1998); http://nsidc.org/data/docs/fgdc/ggd318_map_circumarctic
21. Weedon, G. P. *et al*. *The Watch Forcing Data 1958–2001: A Meteorological Forcing Dataset for Land Surface- and Hydrological-Models* WATCH Technical Report 22 (WATCH, 2010); http://www.eu-watch.org/publications
22. Weedon, G. P. *et al*. The WFDEI meteorological forcing data set: WATCH forcing data methodology applied to ERA-interim reanalysis data. *Wat. Resour. Res.* **50,** 7505–7514 (2014).
23. Goodrich, L. The influence of snow cover on the ground thermal regime. *Can. Geotech. J.* **19,** 421–432 (1982).
24. Nelson, F. E. Permafrost distribution in central Canada: applications of a climate-based predictive model. *Ann. Assoc. Am. Geogr.* **76,** 550–569 (1986).
25. Taylor, K. E., Stouffer, R. J. & Meehl, G. A. *A Summary of the CMIP5 Experiment Design* PCMDI Tech. Rep. (WCRP, 2009); http://cmip-pcmdi.llnl.gov/cmip5/docs/Taylor_CMIP5_design.pdf
26. IPCC *Climate Change 2013: The Physical Science Basis* (eds Stocker, T. *et al*.) (Cambridge Univ. Press, 2013).
27. Xie, Y., Liu, Y. & Huang, J. Overestimated Arctic warming and underestimated Eurasia mid-latitude warming in CMIP5 simulations. *Int. J. Climatol.* **36,** 4475–4487 (2016).

28. Center for International Earth Science Information Network, Columbia University, International Food Policy Research Institute, The World Bank, & Centro Internacional de Agricultura Tropical *Global Rural-Urban Mapping Project, Version 1* (*grumpv1*): *Population Density Grid* (NASA Socioeconomic Data and Applications Center, 2011); http://dx.doi.org/10.7927/H4R20Z93
29. Balk, D. *et al*. Determining global population distribution: methods, applications and data. *Adv. Parasitol.* **62,** 119–156 (2006).

Acknowledgements

The authors acknowledge funding and support from the Permafrost in the Arctic and Global Effects in the 21st century (PAGE21) Framework 7 project GA282700. S.E.C., G.H. and S.W. were funded under the Joint Partnership Initiative (JPI) project COnstraining Uncertainties in the Permafrost-climate feedback (COUP) (S.E.C.: National Environment Research Council grant NE/M01990X/1; G.H.: Swedish Research Council grant no. E0689701; S.W.: Research Council of Norway project no. 244903/E10 with additional funding for S.W. through SatPerm and Permanor (Research Council of Norway project no. 239918 and 255331/E10)). E.J.B. was supported by the Joint UK DECC/Defra Met Office Hadley Centre Climate Programme (GA01101). P.M.C. and P.F. acknowledge funding from CRESCENDO (EU project 641816). S.E.C. is grateful to the University of Exeter for access to facilities. Thanks to D. Pearson for helpful discussions, and A. Lebéhot for comments on the manuscript.

Author contributions

S.E.C. developed the techniques, made the calculations for future projections of permafrost, and produced the plots and manuscript. S.W. and G.H. provided and analysed data for evaluation, along with advice and comments. E.J.B. extracted CMIP5 model data. P.M.C. came up with the original idea to address this question. P.M.C., E.J.B. and P.F. provided advice, ideas and discussion throughout the process. All authors contributed towards writing the manuscript.

Additional information

Supplementary information is available in the online version of the paper. Reprints and permissions information is available online at www.nature.com/reprints. Publisher's note: Springer Nature remains neutral with regard to jurisdictional claims in published maps and institutional affiliations. Correspondence and requests for materials should be addressed to S.E.C.

Competing financial interests

The authors declare no competing financial interests.

Methods

Deriving the relationship between permafrost and MAAT for observations. The relationship shown in Fig. 1a is produced by combining the International Permafrost Association (IPA) map[20] with WATCH reanalysis air temperature data at 0.5° spatial resolution[21,22]. The IPA map defines the boundaries of the permafrost zones: continuous, >90% coverage; discontinuous, 50–90% coverage; sporadic, 10–50% coverage; isolated patches, 0–10% coverage. We extracted the grid cells from WATCH that corresponded to the spatial boundaries of these permafrost zones on the IPA map, and also any grid cell within 100 km of the boundary to account for uncertainties in the boundary placement or in fractional coverage at the boundaries. We used 31 years of mean annual air temperatures (1960–1990), corresponding to the approximate time period from which the information in the IPA map was compiled. We took a 5-year rolling mean of the air temperatures to remove some of the interannual variability, since permafrost responds on a multi-annual timescale. The air temperature data were fitted against the permafrost fractions at the corresponding zonal boundaries (0%, 10%, 50% and 90%). The curve was fitted using least-squares regression, and taking the same functional form as in ref. 19, with two free parameters. The curve follows cumulative normal distribution functions (that is, a predefined shape). However, in ref. 19 only the 10% and 90% points are fixed using literature values. Note that our curves are based on a much larger number of permafrost fraction versus MAAT points that are obtained from the IPA permafrost map. Furthermore, these points cover a range of possible values from 0 to 90%, so that our estimates are well constrained. See the Supplementary Methods for a detailed validation of this relationship against observations and high-resolution modelling.

Due to their coarse resolution the 0.5° air temperatures do not resolve the southern mountain ranges in Europe and North America and therefore show permafrost at a MAAT up to +14 °C, at which it certainly cannot exist, so we removed these mountain ranges from the IPA map before fitting the curves.

The upper and lower curves in Fig. 1a were derived by binning the grid cells according to air temperature (1 °C intervals) and taking the permafrost fractions for each grid cell in each bin. In each air temperature bin, we took the upper 50% of permafrost fractions to fit the upper curve, and the lower 50% to fit the lower curve. While this does not place the curves at the absolute extremes of the data, it well captures the large-scale variability, as shown in Fig. 1 and further in Supplementary Information.

Permafrost area from the IPA map. The total permafrost area from the IPA map[20] was estimated by assuming the fractional coverage in each permafrost zone falls at the centre of the zonal range. The upper and lower bounds were estimated by assuming the maximum/minimum fraction in all zones.

Analysis of CMIP5 models. Model-specific relationships between MAAT and permafrost were estimated for the CMIP5 models[25]. These were derived by taking a set of points from each model grid, at 2° latitude/longitude intervals north of 50° latitude, and splitting these according to 1 °C intervals of MAAT. In each air temperature interval we calculated the fraction of points at which permafrost was simulated. For consistency with the observations, we took these values from the historical simulations from 1960–1990. The limiting curves were estimated by taking the 50% of points with the warmest and coldest soil temperatures for a given MAAT interval. This is very similar to the derivation of upper and lower bounds for the observed relationship, except that in the observations only the permafrost fraction is known, whereas in the models only a single soil temperature is simulated for each grid cell.

The MAAT–permafrost curves for the CMIP5 models (equivalent to Fig. 1a) are shown in Supplementary Fig. 3. The variety of different MAAT–permafrost relationships show the discrepancies in model representations of permafrost due to the inclusion/neglect of such processes as snow insulation, thermal inertia and latent heat. This results in relative curve shifts of up to 10 °C, and curve gradients that vary from almost vertical to very shallow curves (for example, NorESM1).

For future assessments we used the models that run stabilizations to 2300 for RCP4.5 and RCP2.6. We do not include RCP8.5 in this analysis: firstly there are very few CMIP5 models that ran to 2300 with RCP8.5, and almost exclusively the warming is so high in these runs that there is no permafrost remaining, which prevents further analyses of the MAAT–permafrost relationship.

To use our approach, it is important that the same relationships apply under equilibrium conditions, and we verify this in the models on Supplementary Fig. 4, where we plot the MAAT–permafrost curves at stabilization at 2300, along with those derived from the historical simulations from 1960–1990. In fact, there are some small differences in some of the models, but these are also the models with the largest uncertainty bounds on the curve and thus the relationships at equilibrium fall within the plausible range.

Projection of future air temperatures. To estimate the future air temperatures we increased the historical air temperatures by the global mean warming, multiplied by an Arctic amplification factor. The amplification factor was derived as a function of latitude, via a regression of air temperatures over land, in 5° latitude bands, against the global mean air temperature, using WATCH reanalysis air temperature data from 1936 to 2012[21,22].

The base air temperatures from which the air temperatures for different scenarios are derived, using this pattern-scaling approach, are taken from the WATCH 1986–2005 20-year mean. At this time global warming is assumed to be 0.61 °C (ref. 26).

The Arctic amplification uncertainty was estimated using the CMIP5 models, by comparing the amplification factors in their historical simulation with their future simulation. By combining all the models together we derived a full spatial covariance matrix of uncertainties.

Uncertainties for the final constraint were combined from taking upper and lower curves from the permafrost–MAAT relationship, and from the Arctic amplification covariance matrix. For the permafrost–MAAT curves we cannot calculate the spatial covariance, so we assume the maximum (minimum) permafrost area is when every grid cell falls on the upper (lower) curve. To combine with the amplification uncertainties, we assume that these limits correspond to 2σ. This approach gives an upper limit on the uncertainty: while the permafrost–MAAT relationship varies locally and for a given location it can shift under climatic changes (for example, drier summers), the chances that it will fall on either the upper of lower curve across the whole Arctic are extremely small. We include such variability in the uncertainty bounds rather than explicitly resolving it, because the future changes and even the present-day variability (since, for example, sub-surface characteristics are not recorded in detail on global scales) are not yet well understood. The sensitivity of permafrost to warming, and corresponding uncertainty bounds, were calculated from the 2° stabilization relative to pre-industrial levels.

The future Arctic amplification is subject to large uncertainties. Supplementary Fig. 5 shows the amplification factors as a function of latitude in the models and observations, over the same historical period. The historical amplification factor derived from the air temperature record is qualitatively different from in most models[27] (Supplementary Fig. 5), suggesting that models may be failing to represent or misrepresenting some processes. On the other hand, observations are sparse in the very high latitudes, so it may arguably be more reliable to use models for this region. In practice, since models and observations overlap in the very high latitudes, it does not make a large difference whether we choose to use the observed or simulated values. We argue that while observations are sparse, they are less likely to have a consistent bias, which the models clearly have since they consistently disagree with the observations in the mid-northern latitudes, where observed data are quite reliable. Therefore, we choose to estimate the future Arctic amplification from historical observations, but to use the models to give statistical uncertainty bounds (using spatial covariance of future amplification).

It has been argued that Arctic amplification in future may be larger than over the last century, since it has been suppressed over the last century by aerosol effects[30]. Conversely, under very high warming scenarios, sea ice and snow could largely disappear from the Arctic, leading to a reduction in the albedo feedbacks and thus a reduced amplification effect. The future of permafrost under the high warming scenarios is therefore uncertain (see Fig. 3). Further studies of Arctic amplification in palaeoclimate records may enable this constraint to be tightened[31].

Data availability. The data sets analysed during the current study are available online: WATCH reanalysis data: http://www.eu-watch.org/data_availability; IPA permafrost map: https://nsidc.org/data/ggd318; CMIP5 model outputs: http://cmip-pcmdi.llnl.gov/cmip5/availability.html. The data sets generated during the study, in particular the estimated permafrost maps, are available in the PANGAEA repository, at https://doi.org/10.1594/PANGAEA.873192. Parameters used in generating the maps are included in Supplementary Fig. 1 and Supplementary Table 2. Any further data, such as uncertainties for estimating future air temperatures, are available from the corresponding author on reasonable request.

References

30. Shindell, D. & Faluvegi, G. Climate response to regional radiative forcing during the twentieth century. *Nat. Geosci.* **2,** 294–300 (2009).
31. Miller, G. H. *et al*. Arctic amplification: can the past constrain the future? *Quat. Sci. Rev.* **29,** 1779–1790 (2010); Special theme: Arctic palaeoclimate synthesis (1674–1790).